# Contact effect in the dynamic electron transport of a two-probe mesoscopic conductor*

Quan Jun(全 军), Xiao Shi-Fa(肖世发), and Tian Ying(田 英)†

*School of Physics Science and Technology, Zhanjiang Normal University, Zhanjiang* 524048, *China*

(Received 16 January 2013; revised manuscript received 22 February 2013)

Based on the self-consistent electron dynamic transport theory for multi-probe mesoscopic systems, we calculate the distribution of internal potential, charge density, and ac conductance of a two-probe mesoscopic conductor with wide trapezoid reservoirs, and study the contact effect. The results show that including the contact effect can make a significant difference to the frequency-dependent electron transport properties. In the nonzero frequency case, the internal potential and the charge density are complex with extremely small imaginary parts. Importantly, the imaginary part of the charge density gives rise to a real ac conductance (admittance), which corresponds to the charge-relaxation resistance.

**Keywords:** mesoscopic system, electron transport, conductance, charge density

**PACS:** 73.23.–b, 73.40.–c **DOI:** 10.1088/1674-1056/22/7/077304

## 1. Introduction

The study of time-dependent electron transport in mesoscopic conductors is a rapidly developing field of research.[1–11] One of the studied systems is a one-dimensional (1D) structure connected to wide reservoirs which are biased with frequency-dependent voltages; in this case, the electron–electron (e–e) interaction plays a key role in ensuring the charge (current) conservation and the gauge invariance under potential shifts.[12–14] In view of the e–e interaction, Büttiker *et al.*[1,3,5,6] have developed an electron transport theory for mesoscopic systems by employing continuous and discrete internal potential models; this is an important advance in mesoscopic physics and warrants further development. Blanter *et al.* adopted the random phase approximation (RPA) to calculate the ac conductance in the presence of the e–e interaction.[15] Sablikov *et al.* used the Hartree–Fock approximation to investigate the internal potential and electron-density distributions in a quantum wire.[16] Sablikov and Polyakov studied the one-dimensional e–e interaction using the Bosonization technique.[17] Hence, the frequency-dependent conductance, the internal potential, and the electron-density distributions in mesoscopic systems have been investigated under low-frequency conditions. However, possible applications of mesoscopic electronic devices in future all involve higher frequencies; then the detailed knowledge of the time-dependent transport properties of mesoscopic structures is required. The front say, the e–e interaction, and the electronic coherence have been shown to be important in time-dependent mesoscopic transport. In the preliminary studies, the e–e interaction is frequently treated under low frequencies or modeled by introducing a frequency-independent geometric capacitance.[1,3,5] In addition, in the transition region from a macroscopic lead to the mesoscopic transport system, there exists a contact region composed of macro leads and nanostructures. The accumulation favorites of electrons have significant effects on the transport properties of the system, hence, the contacts also play an important role in the conductance due to its significant interaction with the conductors.[13–15,18,19] However hitherto the effect of contacts on the ac transport in a mesoscopic structure has not yet been further investigated. In this paper, a two-probe mesoscopic conductor with trapezoid contacts is studied, as shown in Fig. 1, we will discuss the effect of contacts on the internal potential, charge density, and frequency-dependent conductance.

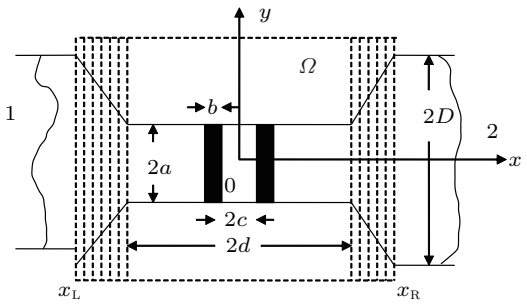



**Fig. 1.** Schematic diagram of a two-probe mesoscopic conductor with two trapezoid reservoirs, $|x_L| = x_R = L$.

## 2. Model and theory

The model we consider here is shown schematically in Fig. 1. Two large reservoirs (contacts) occupy the left and the right half-spaces of the $x$–$y$ plane, $x < -d$ and $x > d$, respectively, and a conductor of double-barrier structure of length

*Project supported by the National Natural Science Foundation of China (Grant No. 11147152), the Natural Science Foundation of Guangdong Province, China (Grant No. S2011040002130), and the Youth Program of Zhanjiang Normal University, China (Grant No. L0702).

†Corresponding author. E-mail: rgquan0224@gmail.com

© 2013 Chinese Physical Society and IOP Publishing Ltd 

$2d$ centers on the $x$ axis. The dashed line box labeled by $\Omega$ in Fig. 1 includes the whole conductor and parts of the reservoirs, and it is large enough to cover all the regions with varying distributions of potential and charge. This means that all the electric-field lines come from and end at the charge inside $\Omega$. Then, the width of the trapezoid contact, namely the transition regions between the reservoirs and the 1D leads, can be written as

$$|w(x)| = \begin{cases} 2D, & |x| \geq L, \\ 2\left|\dfrac{D-a}{L-d}(|x|-L)+D\right|, & d \leq |x| \leq L, \\ 2a, & |x| \leq d. \end{cases} \quad (1)$$

To proceed, we assume that the electrons in the system are confined by hard-wall boundaries along the $y$ direction but allowed to move along the $x$ direction, then the transverse eigenstates with eigenvalues given by

$$\varepsilon_l = \frac{l^2\pi^2\hbar^2}{2m_{\rm e}^* w^2(x)}, \quad l = 1,2,3,...$$

in the system read

$$\varphi_l(y) = \sqrt{\frac{2}{|w(x)|}} \sin\left(\frac{l\pi}{|w(x)|}\left(y+\frac{w(x)}{2}\right)\right), \quad (2)$$

where $l$ refers to the transverse mode number, and $m_{\rm e}^*$ is the effective mass of electrons. Hence the scattering wave functions corresponding to the incident electrons with given energy $E$ and wave number

$$k_l = \sqrt{2m_{\rm e}^*(E-\varepsilon_l)/\hbar^2}$$

from the left electron reservoir 1 are given by

$$\begin{aligned} \psi_{1l}(x,y) &= (\mathrm{e}^{\mathrm{i}k_l x} + s_{{\rm LL},ll}\,\mathrm{e}^{-\mathrm{i}k_l x})\varphi_l(y) \\ &= \chi_1^l(x)\varphi_l(y), \quad \text{for} \quad x < x_{\rm L}. \end{aligned} \quad (3)$$

For the electron in the right electron reservoir, the transmitted wave function is

$$\psi_{1l}(x,y) = s_{{\rm RL},ll}\,\mathrm{e}^{\mathrm{i}k_l x}\varphi_l(y) = \chi_1^l(x)\varphi_l(y), \quad \text{for} \quad x > x_{\rm R}. \quad (4)$$

Divide the trapezoid contacts into a series of narrow layers (see Fig. 1, labeled by $j = 1, 2, 3, \ldots$). The wave function in the $j$-th layer can be expressed as

$$\psi_{1l}^j(x,y) = \sum_{l'} (A_{ll'}^j\,\mathrm{e}^{\mathrm{i}k_{l'}^j x} + B_{ll'}^j\,\mathrm{e}^{-\mathrm{i}k_{l'}^j x})\varphi_l^j(y). \quad (5)$$

We assume that the width change in the trapezoid contacts is so slow that the state hopping is ignored, this leads to

$$\psi_{1l}^j(x,y) = (A_l^j\,\mathrm{e}^{\mathrm{i}k_{l'}^j x} + B_l^j\,\mathrm{e}^{-\mathrm{i}k_{l'}^j x})\varphi_l^j(y) = \chi_1^l(x)\varphi_l^j(y). \quad (6)$$

In the 1D region, the wave function of electron may be expanded as

$$\psi_{1l}^I(x,y) = (A_l^I\,\mathrm{e}^{\mathrm{i}k_{l'}^I x} + B_l^I\,\mathrm{e}^{-\mathrm{i}k_{l'}^I x})\phi_l(y) = \chi_1^l(x)\varphi_l(y), \quad (7)$$

where $I = 1, 2, \ldots$ represent the regions of the two barriers, the well, and the two 1D leads, respectively, $k_l^I = \sqrt{2m_{\rm e}^*(E-U_I)/\hbar^2 - l^2\pi^2/4a^2}$, and $U_I$ is the double barrier potential and given by

$$U_I = \begin{cases} V_0, & \text{in the barriers,} \\ 0, & \text{elsewhere.} \end{cases} \quad (8)$$

Generally, the wave functions need to be matched at the boundaries with the requirement that amplitudes and derivatives with respect to $x$ are equal across the boundaries. By eliminating $s_{{\rm LL},ll}$ and $s_{{\rm RL},ll'}$ from the resulting equations of the matching, the wave functions can be determined.

The scattering wave functions $\psi_{2l}(x,y) = \chi_2^l(x)\varphi_l(y)$ corresponding to the incident from the right electron reservoir 2 can be obtained by replacing $x$ with $-x$. Neglecting the variation of the potential with $y$ and $z$ and assuming that the internal potential function $u_\alpha(\boldsymbol{r},\omega)$ in reservoir $\alpha$ is a function of $x$ only, i.e., $u_\alpha(\boldsymbol{r},\omega) = u_\alpha(x,\omega)$, we obtain the following equation by integrating over $y$ and $z$ and using $\int |\phi_l(\boldsymbol{r})|^2\,\mathrm{d}y\mathrm{d}z = 1$ for the convenience of presentation:[2]

$$\begin{aligned} &\frac{\mathrm{d}^2}{\mathrm{d}x^2}u_\alpha(x,\omega) + \frac{1}{S\varepsilon_0}\int \Pi(x,x',\omega)u_\alpha(x',\omega)\,\mathrm{d}x' \\ &= -\frac{1}{S\varepsilon_0}\rho_\alpha^{\rm ext}(x,\omega), \qquad \alpha = 1,2, \end{aligned} \quad (9)$$

where $S = |w(x)|h$ is the cross-section of the two-probe mesoscopic conductor, and $h$ is the thickness of the system. The $\Pi(x,x',\omega)$ is the so-called Lindhard function

$$\begin{aligned} \Pi(x,x',\omega) &= e^2 \sum_{\gamma,\delta,l,l'} \iint \frac{\mathrm{d}E\,\mathrm{d}E'}{h v_l v_{l'}} \chi_\delta^{l*}(x)\chi_\gamma^{l'}(x)\chi_\gamma^{l'*}(x')\chi_\delta^l(x') \\ &\quad \times \frac{f(E)-f(E')}{E-E'+\hbar\omega+\mathrm{i}\hbar\eta^+}, \qquad \gamma,\ \delta = 1,2, \end{aligned} \quad (10)$$

where $v_l = \sqrt{2(E-\varepsilon_l)/m_{\rm e}^*}$, and $f(E)$ is the Fermi–Dirac distribution function. The $\rho_\alpha^{\rm ext}(x,\omega)$ in the right-hand side of Eq. (9) is the response of charge in reservoir $\alpha$ to the external fields, and reads

$$\begin{aligned} \rho_\alpha^{\rm ext}(x,\omega) &= \frac{e^2}{\hbar} \sum_{\delta,\gamma,l,l'} \iint \frac{\mathrm{d}E\,\mathrm{d}E'}{h v_l(E) v_{l'}(E')} \rho_{\delta\gamma}^{ll'}(x) I_{\gamma\delta}(x_\alpha) \\ &\quad \times \frac{f(E)-f(E')}{(E-E'+\hbar\omega+\mathrm{i}\hbar\eta^+)(E-E')}, \end{aligned} \quad (11)$$

with

$$\rho_{\delta\gamma}^{ll'}(x) = [\chi_\delta^l(x)]^*\chi_\gamma^{l'}(x),$$

where $I_{ll'}^\alpha(x_\alpha)$ can be expressed in terms of the wave functions

$$\begin{aligned} I_{\gamma\delta}(x_\alpha) &= \frac{\hbar}{2\mathrm{i}m_{\rm e}^*}\left\{[\chi_\gamma^{l'}(x)]^*\frac{\partial}{\partial x}\chi_\delta^l(x)\right. \\ &\quad \left. - \chi_\delta^l(x)\frac{\partial}{\partial x}[\chi_\gamma^{l'}(x)]^*\right\} \times \Big|_{x=x_\alpha}, \end{aligned} \quad (12)$$

namely,

$$I_{\gamma\delta}(x_\alpha) = \frac{\hbar}{2\mathrm{i}m_\mathrm{e}}[\delta_{\alpha\gamma}\delta_{\beta\gamma}I^{++}(x_\alpha) + \delta_{\alpha\gamma}S_{\beta\gamma}(E')I^{+-}(x_\alpha) + \delta_{\beta\delta}S^*_{\alpha\gamma}(E)I^{-+}(x_\alpha) + \delta_{\alpha\gamma}S^*_{\alpha\gamma}(E)S_{\beta\gamma}(E')I^{--}(x_\alpha)], \quad (13)$$

with

$$I^{o_1o_2}(x_\alpha) = \mathrm{i}(o_1k_\gamma + o_2k_\delta)\,\mathrm{e}^{\mathrm{i}(o_2k_\delta - o_1k_\gamma)x_\alpha}, \quad o_1, o_2 = \pm 1. \quad (14)$$

Hence, the dynamic response of charge density in the two-probe mesoscopic conductor to the external voltage is[2]

$$\rho_\alpha(x,\omega) = \rho^{\mathrm{ext}}_\alpha(x,\omega) + \int \mathrm{d}x' \Pi(x,x',\omega)u_\alpha(x',\omega). \quad (15)$$

### 2.1. Charge density and internal potential

To solve Eq. (9) for $u_\alpha(x,\omega)$, the following boundary condition is adopted:

$$u_\alpha(x_\alpha,\omega) = \begin{cases} 1, & \alpha = \beta, \\ 0, & \alpha \neq \beta. \end{cases} \quad (16)$$

To make further progress, taking the limit that $\eta^\dagger$ goes to zero and using

$$\lim_{\eta^\dagger \to 0} \frac{1}{x \pm \mathrm{i}\eta^\dagger} = -\mathrm{i}\pi\delta(x) + \mathrm{P}\left[\frac{1}{x}\right], \quad (17)$$

where P indicates a principal-value integral, we have

$$\mathrm{Im}[\Pi(x,x',\omega)] = \frac{e^2}{2\hbar}\sum_{\delta,\gamma,l}\int \frac{\chi^*_\delta(x)\chi_\gamma(x)\chi^*_\gamma(x')\chi_\delta(x')[f(E) - f(E+\hbar\omega)]}{v_l(E)v_l(E+\hbar\omega)}\mathrm{d}E, \quad (18)$$

$$\mathrm{Im}[\rho^{\mathrm{ext}}_\alpha(x,\omega)] = \frac{e^2}{2\hbar^2}\sum_{\delta,\gamma,l}\int \frac{\rho^{ll'}_{\delta\gamma}(x)I_{\gamma\delta}(X_\alpha)}{v_l(E)v_l(E+\hbar\omega)}\frac{f(E) - f(E+\hbar\omega)}{\hbar\omega}\mathrm{d}E. \quad (19)$$

Then the real parts of $\Pi(x,x',\omega)$ and $\rho^{\mathrm{ext}}_\alpha(x,\omega)$ can be obtained by applying the Kramers–Kronig relation, for instance

$$\mathrm{Re}[\rho^{\mathrm{ext}}_\alpha(\omega)] = \frac{2}{\pi}\mathrm{P}\int \frac{v\mathrm{Im}[\rho^{\mathrm{ext}}_\alpha(\omega)]}{v^2 - \omega^2}\mathrm{d}v. \quad (20)$$

In numerical calculation, the length, energy, and conductance are measured in units of the Bohr radius $a_0 = 4\pi\varepsilon_0\hbar^2/m^*_\mathrm{e}e^2$, $\Delta = \pi^2\hbar^2/2m^*_\mathrm{e}a_0^2$, and $e^2/2h$, respectively, and $a = 20$, $b = 0.6$, $c = 0.4$, $d = 2$, $h = 0.1$, $V_0 = 4$. The channel numbers or modes in different regions of the system are $\max[6, 6l_{\max}]$ with $l_{\max} = \mathrm{int}[|w(x)|\sqrt{2m^*_\mathrm{e}E}/\pi\hbar]$. The frequency $\omega$ of the voltage is the normalized value, i.e., $\omega \to \hbar\omega/\Delta$.

We present in Fig. 2 the distributions of charge density for various widths of reservoirs at temperature $T = 0$, $k_\mathrm{F}a = 1$, and $\omega = 0.5$, where $k_\mathrm{F}$ is the Fermi wave number. The results show that the charge driven to the other side of the conductor can penetrate through the barrier with a small probability, namely most of the charge carriers are reflected back into the 1D leads and the reservoir, and there is no charge accumulation beyond the barrier. The figure clearly shows that the charge density increases with the increasing width of the reservoir, particularly in the contact region. This indicates that the contact obviously influences the distributions of charge density. From the curves in Fig. 2 we can conclude that the potential drop appears in the transition region between the 1D lead and the contact, as shown in the inset of Fig. 2.

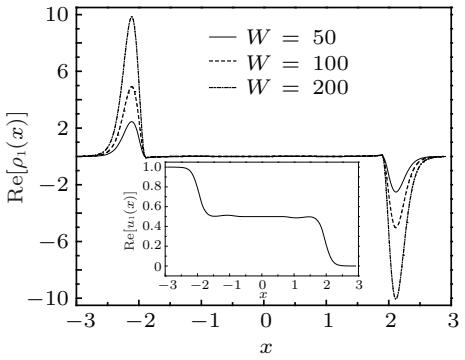



**Fig. 2.** Distribution of real parts of charge and (inset) internal potential.

In the case with $k_\mathrm{F}a = 1$, zero temperature, and $W = 100$, $u_1(x)$ decreases sharply and reaches a plateau in the 1D portion. Note that the distributions of charge and internal potential are complex; compared with the real part, the imaginary part is extremely small, as shown in Fig. 3, but the imaginary part of charge should be taken into account in the following discussion because it gives rise to a real admittance, which actually corresponds to the charge-relaxation resistance.[6]

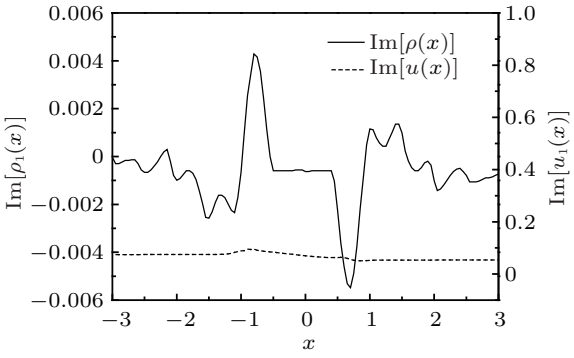



**Fig. 3.** Distribution of imaginary parts of charge and internal potential.

In the case with $T = 0$, $k_\mathrm{F}a = 0.5$, and $\omega = 0.5$, some positive and negative peaks in the charge distribution appear around the barriers, as shown in Fig. 4; they correspond to the junction capacitances produced by the barriers. It is similar to

the results given in Fig. 2, the charge accumulation increases with the increasing width of the reservoir. The internal characteristic potential is shown in the inset of Fig. 4, the potential drop occurs on the left barrier and keeps on 1/2 in the 1D part, and on the right barrier it begins to decrease to zero.

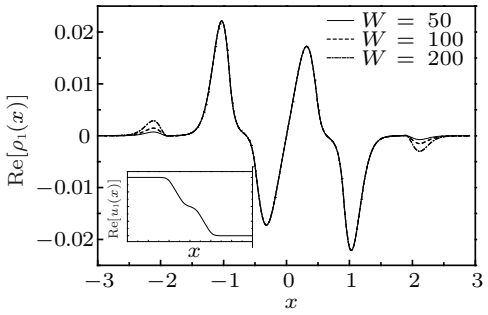



**Fig. 4.** Distribution of real parts of charge and (inset) internal potential.

### 2.2. Frequency-dependent conductance matrix

In the presence of a voltage with frequency $\omega$ applied on the reservoirs, the external conductance matrix with elements corresponding to the current response of the system to the voltage can be written as

$$\mathrm{Re}[G^{\mathrm{ext}}_{\alpha\beta}(\omega)] = \frac{e^2}{2\hbar}\sum_{\delta,\gamma,l}\int \frac{\mathrm{d}E}{v_l(E)v_l(E+\hbar\omega)} \times I_{\gamma\delta}(x_\alpha)I_{\delta\gamma}(x_\beta)\frac{f(E)-f(E+\hbar\omega)}{\omega}, \quad (21)$$

$$\mathrm{Im}[G^{\mathrm{ext}}_{\alpha\beta}(\omega)] = -\frac{2\omega}{\pi}\mathrm{P}\int \frac{\mathrm{Re}[G^{\mathrm{ext}}_{\alpha\beta}(\omega)]}{v^2-\omega^2}\mathrm{d}v. \quad (22)$$

This conductance matrix does not conserve the current, since $\sum_\alpha G^{\mathrm{ext}}_{\alpha\beta}(\omega) \neq 0$, so we must consider the current response to the internal potential, which leads to

$$G^{\mathrm{int}}_{\alpha\beta}(\omega) = \int g_\alpha(x,\omega)u_\beta(x,\omega)\mathrm{d}x, \quad (23)$$

where $g_\alpha(x,\omega)$ is a local current response function, and has the form

$$\mathrm{Im}[g_\alpha(x,\omega)] = -\frac{e^2}{2\hbar}\sum_{\delta,\gamma,l}\int \frac{I^{(}_{\delta\gamma}X_\alpha)\rho^{ll'}_{\delta\gamma}(x)[f(E)-f(E+\hbar\omega)]}{v_l(E)v_l(E+\hbar\omega)}\mathrm{d}E, \quad (24)$$

$$\mathrm{Re}[g_\alpha(x,\omega)] = \frac{2}{\pi}\mathrm{P}\int \frac{v\mathrm{Im}[g_\alpha(x,\omega)]}{v^2-\omega^2}\mathrm{d}v. \quad (25)$$

With the above expressions, the final formula for the total frequency-dependent conductance matrix element of the mesoscopic conductor is given by[2]

$$G_{\alpha\beta}(\omega) = G^{\mathrm{ext}}_{\alpha\beta}(\omega) + G^{\mathrm{int}}_{\alpha\beta}(\omega), \quad \alpha,\ \beta = 1,2. \quad (26)$$

Figures 5 and 6 show the conductance matrix element as a function of the frequency of voltage for various widths of reservoirs at $T = 0$ and $k_{\mathrm{F}}a = 0.5$. Here it should be pointed that the conductance is also complex, the imaginary part refers to the phase difference between the current and the voltage, this means that there are two different responses to the external time-dependent voltage, i.e., inductive-like and capacitive-like, which depend on the sign (plus or minus) of the conductance matrix elements.

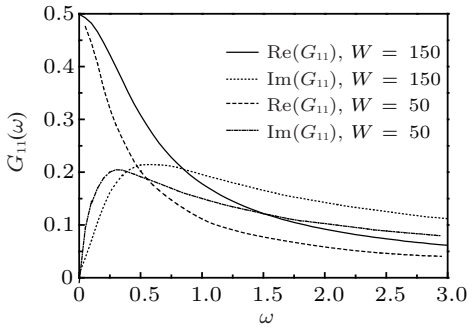



**Fig. 5.** Frequency-dependent conductance matrix element $G_{11}(\omega)$.

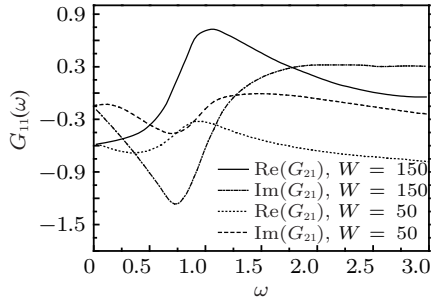



**Fig. 6.** Frequency-dependent conductance matrix element $G_{21}(\omega)$.

In Fig. 5, we can find from the profiles of conductance that the real part of $G_{11}(\omega)$ decreases with the increase of the frequency; the imaginary part of $G_{11}(\omega)$ is nonzero and displays a single-peak structure. And the imaginary part of $G_{11}(\omega)$ is inductive-like.

In Fig. 6, $G_{21}(\omega)$ shows an irregularly oscillation within the region $0 < \omega < 1$, after which it decreases. It is noted that in the time-dependent case, the current distribution is non-uniform due to the e–e interaction. In the low-frequency case, the conductance is capacitive-like; but with increase of the frequency, the inductive-like conductance is observed.

Importantly, by changing the width of the reservoir, a significant difference in the frequency-dependent electron transport properties is found in Figs. 5 and 6, it shows that there exists a quantum coherence between the devices and the contacts in electron transport.

## 3. Conclusion

In conclusion, we have studied the dynamic electron transport properties of a two-probe mesoscopic conductor with wide trapezoid reservoirs, and calculated the charge density,

the internal potential, and the frequency-dependent conductance by including the contact effect in a self-consistent manner. The results show that in the nonzero frequency case, the internal potential and the charge density are complex with extremely small imaginary parts. Compared with the real part, although the imaginary part is extremely small, the imaginary part of charge should be taken into account, because it gives rise to a real admittance, which corresponds to the charge-relaxation resistance. The conductance matrix elements are also complex, the imaginary part refers to the phase difference between the current and the voltage, and its plus–minus corresponds to two different responses to the voltage, i.e., inductive-like and capacitive-like. Importantly, the contact effect is very noticeable.

## References


[1] Büttiker M, Pretre A and Thomas H 1993 *Phys. Rev. Lett.* **70** 4114
[2] Quan J, Tian Y, Zhang J and Shao L X 2011 *Chin. Phys. B* **20** 077201
[3] Büttiker M 1993 *J. Phys: Condens. Matter* **5** 9361
[4] Wang C and Zhang Y H 2006 *Chin. Phys.* **15** 2120
[5] Christen T and Büttiker M 1996 *Phys. Rev. Lett.* **77** 143
[6] Pretre A, Thomas H and Büttiker M 1996 *Phys. Rev. B* **54** 8130
[7] Büttiker M, Thomas H and Pretre A 1994 *Physica B: Condens. Matter* **94** 133
[8] Zhao X A and Chen Y X 2001 *Phys. Rev. B* **64** 085326
[9] Gasparian V, Christen T and Büttiker M 1996 *Phys. Rev. A.* **54** 4022
[10] Ng T K 1996 *Phys. Rev. Lett.* **76** 487
[11] Jauho A and Meir Y 1993 *Phys. Rev. B* **48** 487
[12] Sanchez D and Büttiker M 2004 *Phys. Rev. Lett.* **93** 106802
[13] Spivak B and Zyuzin A 2004 *Phys. Rev. Lett.* **93** 226801
[14] Leturcq R, Sanchez D, Gotz G., Ihn T, Ensslin K, Driscoll D C and Gossard A C 2006 *Phys. Rev. Lett.* **96** 126801
[15] Blanter Y M and Büttiker M 1998 *Europhys. Lett.* **42** 535
[16] Sablikov V A, Polyakov S V and Büttiker M 2000 *Phys. Rev. B* **61** 13763
[17] Sablikov V A and Shchamkhalova B S 1998 *Phys. Rev. B* **58** 13847
[18] Quan J, Tian Y, Zhang J and Shao L X 2011 *Physica B: Condens. Matter* **406** 1607
[19] Yacoby A, Stormer H L, Wingreen N S, Pfeiffer L N, Baldwin K W and West K W 1996 *Phys. Rev. Lett.* **77** 4612